Chapter 3

Functionalized Thermoplastic Poly (urethane-urea) as Hole Conductor for Quantum Dots Sensitized Solar Cell

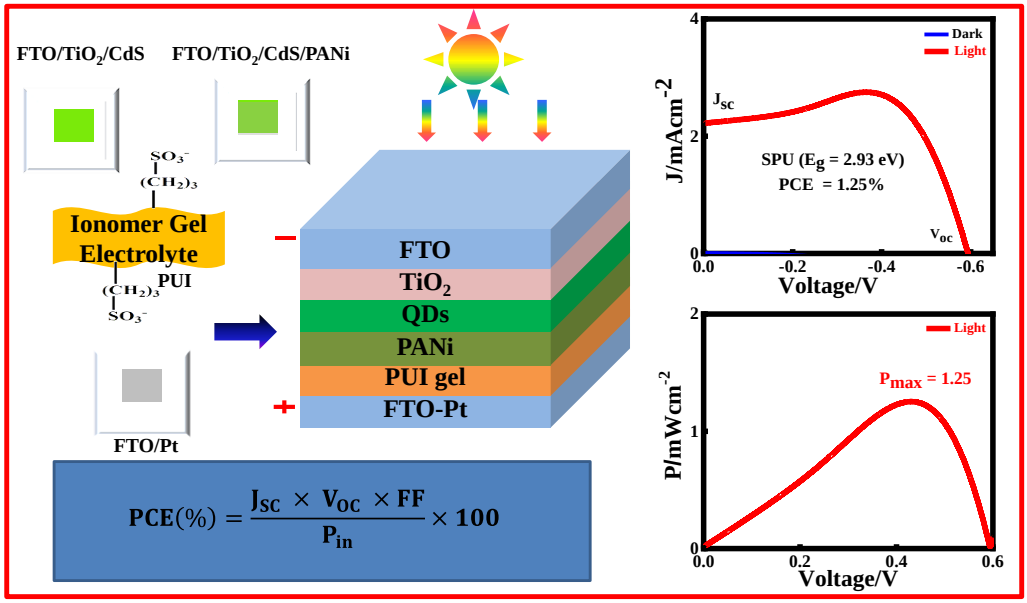

3.1. Introduction

Quantum dots (QDs) of inorganic semiconductor materials have explored as an efficient light absorbing (harvesting) material that generates photoelectrons for the quantum dot sensitized solar cell [117,118]. Continuous solar energy conversion requires reversible charge transport across electrolyte bridge in photovoltaic cell. Electrolytes play a key role in converting solar energy into electrical energy in Quantum dot sensitized solar cell. As functional materials, gel polymer electrolytes are highly efficient towards charge generation and charge transportation. Specific functionalities offer reversibility into polymer network under photo electrochemical influence. Recently, quantum dot sensitized solar cells have been fabricated with various redox electrolytes with different phases i.e., Liquid electrolyte, solid electrolyte, composite electrolyte and gel electrolyte. In most cases, QDSS cells provided degradable performance with liquid electrolyte because of photo corrosion, strong penetration and volatile nature of organic solvents. The undesirable high redox potential of polysulfide/sulfide (S_n^{2-} /S^{2-}) electrolyte have a high overpotential for exciton separation and QD regeneration, Therefore, charge recombination process is intrinsically higher in QDSS cells. The reversible charge transport nature can be realized by chemical functionalization or doping into active content (site) of electrolyte matrix[119]. Further boosting the performance of QDSCs needs the enhancement of photovoltage (Voc) via the adoption of new redox active electrolytes to suppress the charge recombination processes. Gel polymer electrolytes are efficient towards adsorption on photosensitive sites. Polyurethane is completely incompatible with water, which is why a special modification of the backbone is necessary. This is related to the progress in the production of new types of polyurethanes ionomer (polyelectrolyte) with a controlled structure in which polar Ionic groups affecting the phase structure, ionic conductivity and hydrophilicity of polyurethane elastomer. Polyurethanes (PUs) have often been used as matrices for the preparation of ionomers and of polymer

electrolytes [120,121]. Interestingly, ion-containing segmented polyurethanes have found extensive application as useful materials for adhesives, paints, packaging and in the field of electronics i.e. thermal storage devices [97,122]. Polyurethanes are composed of hard segments and soft segments with alternating fashion. They are hydrophobic in nature and insoluble in water [123]. In general, pristine polyurethanes are electrical insulator. Polyurethane hard segments (urethane linkage and urea group) can be functionalized through incorporation of ionic groups or nonionic hydrophilic segments. Therefore, to obtain a stable polyurethane ionomer, sulfonate groups (pendant group) are preferred due to increased hydrophilicity, adhesion and stabilization efficiency [124]. Thus, the semiconducting polyurethanes can be prepared from polyurethane ionomers or hydrophilic polyurethanes. Polar ionic group not only increase the phase separation but also improves thermal resistance (heat storage) of polyurethane ionomer [125,126]. Polyurethane ionomers are non corrosive in nature which causing suitability towards electrolyte activity. The urethane linkages (-NHCOO-) of PU may also enhance the compatibility with PANi through hydrogen bonding. PU ionomers with negatively charged groups may enhance the compatibility with the ES form of PANi through coulombic interactions (anionic groups in the PU backbone interact with the positively charged PANI chains) which may intensify interfacial conductivity[127]. In polyurethane ionomer, the structure is more complex due to the presence of polar anionic segments incorporated by new urethane bonds formed by the reaction of low molecular weight compounds with ion-forming functional groups: usually carboxylic or sulfonic groups in anionomer. The Polyurethane ionomer structure, the method of incorporating ionic segments into the chain determines ionomer properties, including ability to form dispersions in polar solvents, e.g., in water or ionic conductance of formed electrolyte. This is due to the fact that in PU ionomer additional hydrogen bounds and electrostatic interactions are present.

In this study, the electrolyte redox behaviour has been reported by sulfonated polyurethane in QDSS cells. The polyurethanes are composed of hard segment and soft segment in a block fashion. They are hydrophobic in nature. Hydrophilicity of the chains can be enhanced by presence of ionic moiety, which could improve adhesiveness and electrical conductivity. In present scenario, polyurethanes were synthesized through combination of hexamethylene diisocyanates (HMDI), Polytetramethyleglycol (PTMG) and ethylenediamine (EDA). The fascinating structure contains highly active center as urethane linkage (-NHCOO-). The urethane linkage has been functionalized with ϒ-propane sulton. The linked sulfur rich segmented ionomer is expected to be proper hole scavenger in QDSS cell. The electronic structure varies with degree of chemical functionalization. EDTA caped CdS was synthesized to functions as photosensitizer. The quantum dot sensitized solar cell was developed by photocatalyst (TiO_2), Quantum dot (EDTA caped CdS), sulfonated polyurethane ionomer and platinum (Pt). Thus, device contains a layer structure i.e., FTO/TiO_2/CdS/SPUIG/Pt/FTO. In other words, device is composed of photoanode (FTO/TiO_2/CdS), redox electrolyte (SPU) and photocathode (Pt/FTO). Electron – hole pairs were generated by photosensitization. Thin film of PANi has been inserted between photoanode and ionomer electrolyte matrix to intensify interfacial conductivity. The hole conduction was facilitated by inserting a small pendant group into urethane linkage of native polyurethane. The compositions of pendant groups were controlled chemically on hard segment content to establish highly efficient HOMO-LUMO energy levels. Highly functionalized polyurethane was developed as gel electrolyte (matrix). Ionic conductions were generated with functionalized hard segment content. Finally photovoltaic properties were measured by varying electrolyte or different sulfonated polyurethane. Sulfonated polyurethane can be utilized as hole conductor or redox electrolyte for efficient and sustainable photosensitization in quantum dot sensitized solar cell. Efficient functioning

behaviour has been observed due to reduction of extent of charge recombination towards ionomer matrix.

3.2. Results and Discussion

3.2.1. Pendant group and its interaction with hard segment contents of polyurethane chain

Poly (urethane-urea) has been synthesized via reaction of Polytetramethyleneglycol (PTMG), Hexamethylene diisocyanates (HMDI) and ethylene diamine with molar ratio of 1: 5.7: 4.7 at hard segment content of 30%. The reactive –NH group (in urethane and urea) have been functionalized with ϒ – propane sultone to produce ionomeric content in polyurethane chain. The synthesis protocol and reaction scheme is shown in **Scheme 3.1**. Pendant group is a group of atoms or small chain attached on polymer backbone cohesively. Here ϒ- propane sultone acts as ionic pendant group on hard segment contents of polyurethane chain. In other words, sulfonated polyurethanes have been developed through variation of sulfonating agent (ϒ- propane sultone) with constant content of NaH at reaction conditions (60°C, 3h.). Degree of sulfonation varies with extent of interaction of ϒ-propane sultone with hard segment contents (-NHCOO-, -NHCONH-) of polyurethane chain. In ^{1}H NMR spectra **(Figure 3.1a)**, polyurethane showed chemical shift values δ = 5.79 -7.04 ppm due to presence of –NH(a') group of urethane linkage (-NHCOO-) while very week intense peak was observed at chemical shift value δ = 8.20 ppm for –NH(a) proton in urea linkage of polyurethane chain. The alkyl protons showed δ = 0.77 - 1.50 ppm and 4.49 ppm because of presence of HMDI and PTMG (-OCH_2) unit. However, new peaks appeared at δ = 2.48(d), 2.36(b) and 1.70(c) ppm confirmed presence of alkyl sulfonate protons -CH_2(b)-CH_2(c)-CH_2(d)-SO_3^- from ϒ-propane sultone in polyurethane chain. The peak intensity of urethane proton disappeared which indicates that most of the urea groups have been sulfonated with ϒ-propane sultone. However, the chemical shifts δ = 8.33 ppm indicates urethane groups have been sulfonated in

polyurethane chain. The downfield chemical shift values are assigned for reduced hydrogen bonded urethane proton.

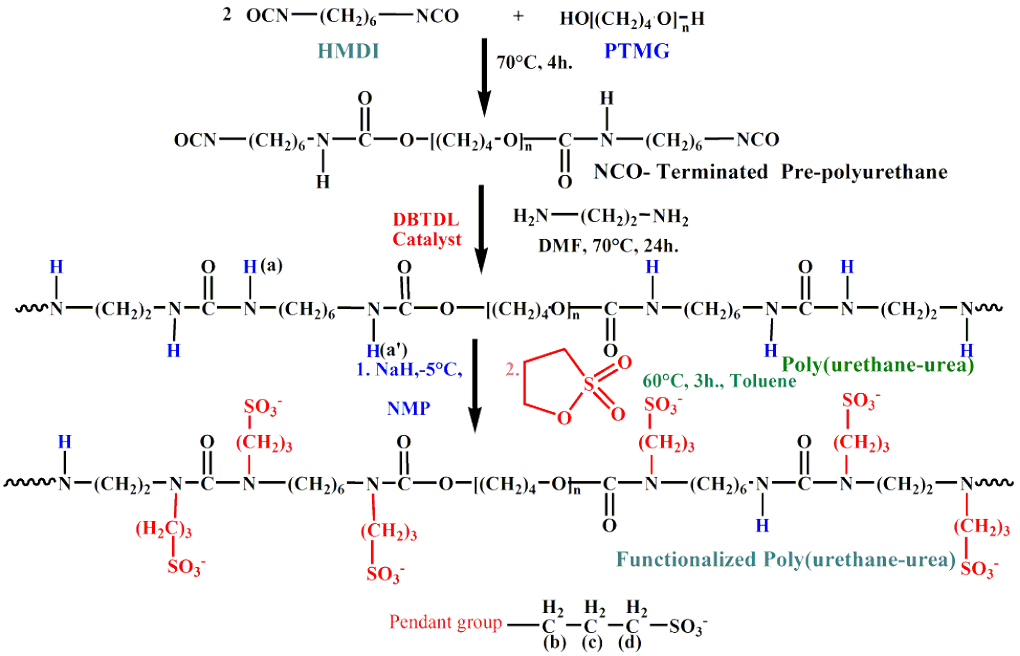

Scheme 3.1 Schematic reaction mechanism of polyurethane synthesis and its chemical functionalization

FTIR spectrum **(Figure 3.1b)** shows direct evidence of interaction of ϒ – propane sultone with hard segment contents of polyurethane chain. Peak intensity varies with concentration of Y- propane sultone or number density of pendant group in polyurethane chain [128]. Pristine polyurethane exhibited a sharp peak with stretching frequency around 3341 cm^{-1} due to presence of hydrogen bonded -NH moiety in urethane or urea group [129]. The stretching frequencies 1621 and 1696 cm^{-1} were assigned for peeks of urethane and urea carbonyl, respectively. The peak at 1569 cm^{-1} is attributed to the bending vibration of –NH group. The peaks at 1109 cm^{-1} are due to the antisymmetric vibration of C–O–C. All these data confirms the formation of urethane group in polyurethane chain. On other hand, broad band appeared at 3396 and 3425 cm^{-1} are attributed to the –NH moiety in SPU-2 and SPU-3, respectively. The shift of wavenumber towards higher values confirms the reduction of H-

bonding of –NH group with carbonyl. The –NH band become more broader and week intense as the concentration of sulfonating agent or number density of pendant group increase on polyurethane hard segment contents [130]. The C=O band in the region of 1650-1750 cm^{-1} is split into two peaks; that centered at lower region is due to bonded C=O, and that at higher region to free C=O, both peaks have close intensity[131]. The stretching frequency of urethane or Urea C=O increases towards higher wavenumber which also confirms the reduction of extent of H- bonding [132]. The peak appeared at 1720 and 1662 cm^{-1} are assigned for C=O frequency in SPU-1. In SPU-2, the peaks appeared at 1726 cm^{-1} is assigned to free C=O group while 1638 cm^{-1} is attributed due to more interaction of sulfonating agent. The wavenumber (frequency) shifts towards higher values as compared to frequency (1691 cm^{-1}) of H- bonded C=O of pristine polyurethane chain. In addition, a intense peak appeared at 1187 cm^{-1} is assigned to sulfonic group S=O group in SPU-3. Thus, all the spectral data confirms the interaction of ϒ – propane sultone with hard segment contents.

Figure 3.1c indicates the TEM micrograph of SPU-3 in thin film phase.. Image clearly maintains the phase separated structure. Polar ionic group, urethane linkage (hard segments) and soft segment forms interconnected structure. It resembles that incorporation of ionic moiety lowers the surface energy result in formation of spherical particle [133].

XRD spectrum of PU shows a hallow diffraction pattern with no sharp peaks has been observed in the pure controlled films thus indicating its amorphous nature. A typical diffraction pattern has been presented in **Figure 3.1(d)**. Polyurethane shows diffraction angle 2Θ = 20.33° for most broad peak. The observed patterns of the crystalline peaks in the 2Θ range are indexed as 23.82°, 21.90°, 21.82°, and 22.17° for the intense peaks in SPU-1, SPU-2, SPU-3 and SPU-4, respectively. The diffraction pattern of SPU-2 and SPU-3 films shows similar type of result with comparatively less intense peaks in the same region. Higher peak

intensities leads us to conclude that sample present the higher chain orientation degree. SPU-4 shows more interaction of ϒ – propane sultone with hard segment content of polyurethane chain leading to more crystallization because of more cross linked structure which favours intensive and intra hydrogen bonding.. The degree of crystallinity changes by varying chain structure or by increasing number density of pendant group or concentration of ϒ- propane sultone on polyurethane chain [134]. The interaction of cation (Na^+) with the ether group of PTMG separates the cation and anionic segments which enhances the amorphous content [135].

Thermogravimetric analysis (TGA) differentiates the heat resistance property in polyurethane and sulfonated polyurethane with reference to polarity difference [136]. TGA curves have been shown in **Figure 3.1e**. The ionomers were found to be less stable in the initial stages (i.e., between 80°C and 135°C), and this is possibly due to the moisture absorbed by the ionomers as the compounds are highly hygroscopic. The polar ionic groups have large capacity to absorb heat. The degradation temperature was estimated at 5% weight loss or 95% confidence limit. Generally, the temperature at which weight loss reaches to 5% is assigned to be the degradation temperature (Td). The stage of degradation of the polyurethane at about 342°C was a result of the depolymerization of the urethane groups. The initial stages of degradation involve random scission degradation of the weaker C-O bonds in block and random structures [137]. Two stage degradation occurred for hard segment and soft segment content in polyurethane chain. The hard segment content becomes more polar upon functionalization withy ϒ – propane sultone. The decomposition temperature 257°C, 242°C, 231°C and 127°C were attributed to the splitting-off of hydrophilic (sulfonate group) at hard segment content of SPU-1, SPU-2, SPU-3 and SPU-4, respectively. However, soft segment decomposition (C-C bonds breaking) > 300°C occurred for all the series of SPU while pristine PU shows soft segment degradation around > 400°C. As the content of ϒ – propane

sultone increases on polyurethane chain, degradation temperature lowered down. However, polar ionic groups contributed to better heat-resistant performance [129,138].

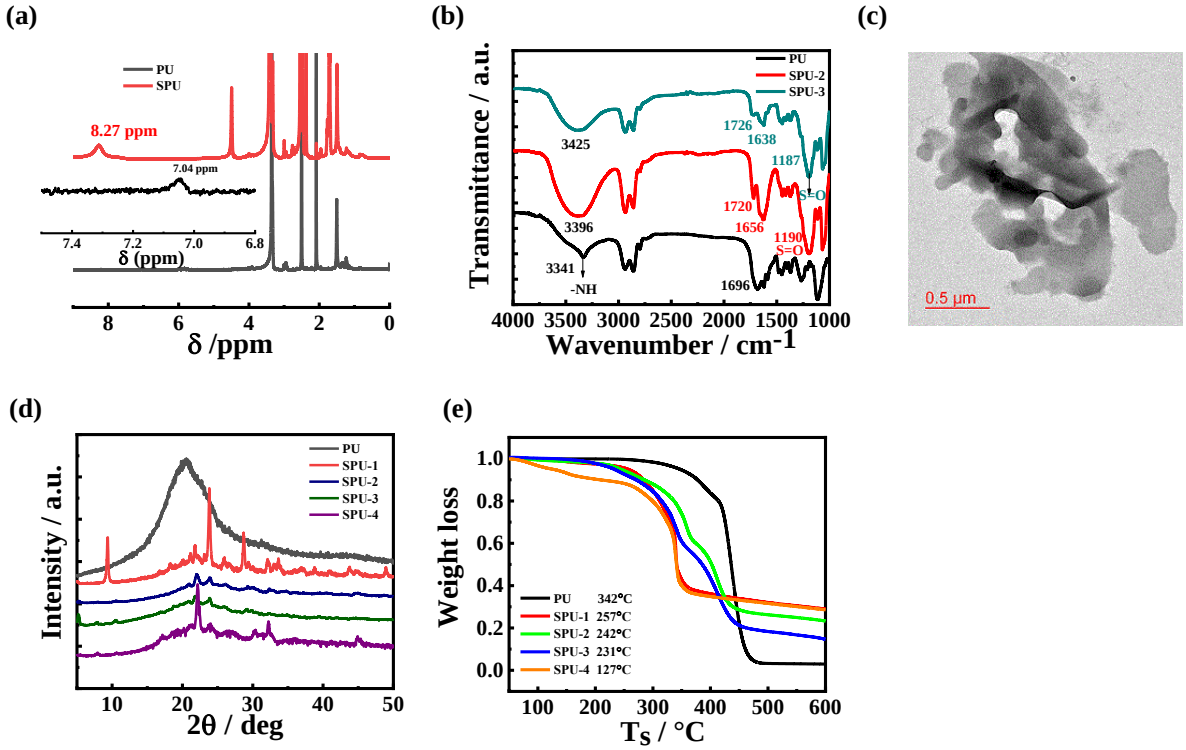

Figure 3.1: (a) ^{1}H NMR investigation for polyurethane and its functionalized matrix. The spectra were recorded after dissolving the sample in d_6-DMSO solvent. **(**b) FTIR study of polyurethane and its functionalized matrixes. FT-IR spectra shows that the intensity of stretching frequency increases with degree of sulfonation and interaction. (c) TEM image of SPU-3 film. (d) XRD pattern of polyurethane urea film and its functionalized structure. (e) Thermogravimetric analysis of polyurethane and sulfonated polyurethane at various level of functionalization.

UV-visible absorption spectrum (**Figure 3.2a**) of poly (urethane – urea) shows two strong absorption peaks at 255 and 221 nm. While the peak at 255 nm is attributed to n → π* excitation absorption due to polar chromophoric (urethane or urea group) transition, the peak at 221 nm is due to π → π* transition in the carbonyl group of hard segment content. When polyurethane (PU) functionalized with ϒ – propane sultone (SPU-1), n → π* transition shifted towards longer wavelength 271 nm predominantly. The shifting of absorption peak confirmed the interaction of hard segment contents with new additional chromophoric

content or alkyl sulfonate group (pendant group) from ϒ – propane sultone. The n → π* transition more shifted towards longer wavelength as the concentration of sulfonating agent increases. The SPU-2, SPU-3 and SPU-4 show absorption peaks at 298, 316, 348 nm, respectively. UV-visible spectra of SPU-2, SPU-3 and SPU-4 depict extensive absorption of light due to expansion of peaks. The peaks become broader due to enhanced dipole –dipole interactions of alkyl sulfonated with rest of the polyurethane chain. Thus, alkyl sulfonate improves the absorption behaviour of polyurethane. The pendant group shifts the HOMO-LUMO energy levels of polyurethane ionomer due to structural or quantum confinement effects.

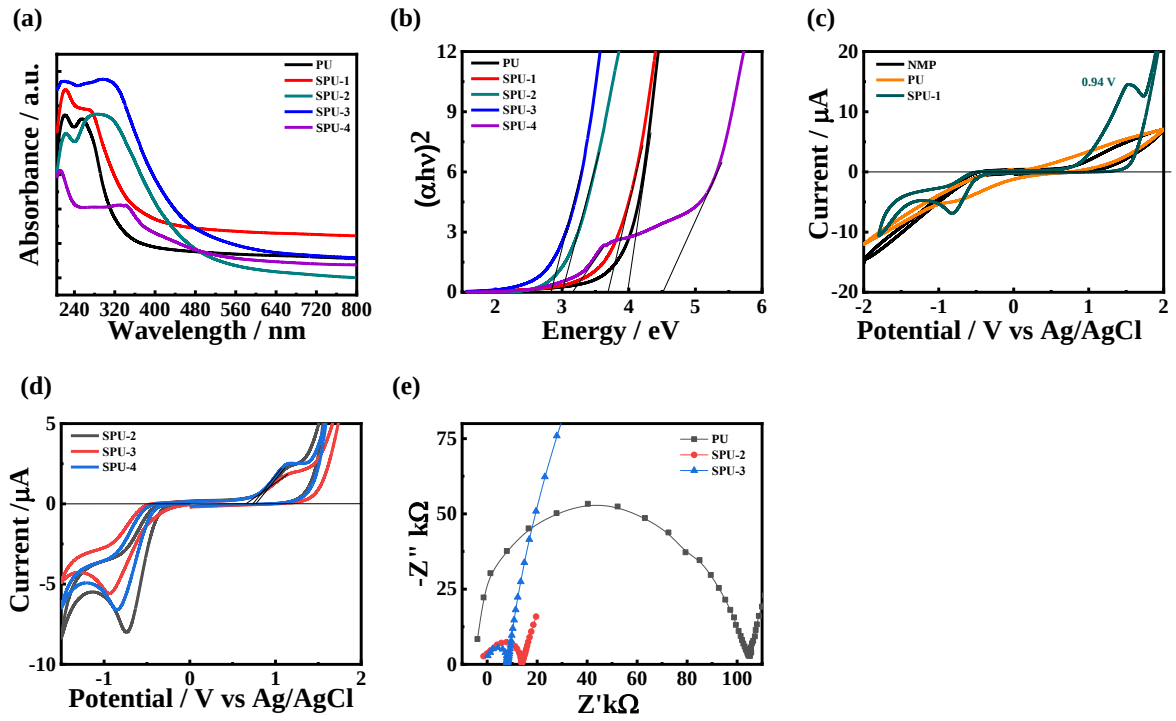

Figure 3.2: Polyurethane and its functionalized matrix: sulfonation at hard segment content with variation of sulfonating agent. (a) UV-visible spectra of pure PU and SPUs with variable content of sulfonating agent. (b) Determination of energy gap (Tauc's plot) from absorption edge transition. (c) Solution phase cyclic voltammetry of solvent NMP, PU and SPU-1 with scan rate of 20 mV/s at room temperature. (d) Cyclic voltammetry of SPU-2, SPU-3 and SPU-4. (e) EIS measurement solution phase PU, SPU-2 and SPU-3 for the measurement of charge transfer resistance.

The Tauc's plot **(Figure 3.2b)** shows direct measurement of energy gap between HOMO and LUMO. The physical parameters are listed in **Table 3.1**. The direct energy gap 4.01, 3.75, 2.98, 2.93 and 3.15 eV have been estimated for PU, SPU-1, SPU-2, SPU-3 and SPU-4, respectively. However, very high concentration of sulfonating agent slightly increases the energy gap of polyurethane ionomer. This exclusive change can be rationalized with enhancement of intra-repulsion force (ionic-dipole and dipole - dipole interactions) among anionic pendant groups. Moreover, the increase in band gap arises due to structural relaxation into polyurethane chain.

Sample	Weight ratio of sulfonating agent	λ_{max} (nm)	E_g (eV)	E_{ox} (V)	HOMO (eV)	LUMO (eV)
PU	0.0	255	4.01	-	-	
SPU-1	0.11	271	3.75	0.94	-5.34	-1.59
SPU-2	0.25	298	2.98	0.77	-5.17	-2.19
SPU-3	0.36	316	2.93	0.66	-5.06	-2.13
SPU-4	0.50	348	3.15, 4.49	0.73	-5.13	-1.98, -0.94

Table 3.1: Calculation of HOMO-LUMO energy levels with UV-visible absorption spectra and electrochemical cyclic voltammetry measurement in the window of –2V to +2V.

3.2.2. Electrochemical characteristic response of polyurethane ionomer

Cyclic voltammetry curve **(Figure 3.2c,d)** showed stability in polyurethane chain and confirmed the redox inactive behaviour at room temperature. However, sulfonated polyurethane exhibits clear sign of oxidation and reduction peaks. The reversible curve does not show any phase transition in potential range. The potential of anodic peak sifted significantly as the degree of ionization or sulfonate group increased on polyurethane hard segments. The onset potential of anodic peak appeared at 0.94V (vs Ag/AgCl) with scan rate of 20 mV/s which confirmed the attachment of redox active pendant group in hard segment contents of SPU-1. The onset anodic potential appeared around 0.77, 0.66 and 0.73V in SPU-2, SPU-3 and SPU-4. The anodic potential shifted little larger in SPU-4 as compared to SPU-3. The high concentration of sulfonating agent can cause aggregation in hard segments due to

physical cross link. The larger value is ascribed with more activation energy of redox active unit in aggregated phase of SPU-4. Thus, shift in potential depends on ion content and hard segment contents in polyurethane ionomers.

Figure 3.2e shows Nyquist plot (EIS measurements) for solution phase PU, SPU-2 and SPU-3. The plot showed large semicircle for Poly (urethane-urea) solution with charge transfer resistance (R_{CT} = 1.10×10^5 Ω. The corresponding ionic conductivity was estimated as 36.5×10^{-5} S/cm. However, functionalized polyurethanes showed reduced size of semicircle confirming lower charge transfer resistance and hence enhanced ionic conductivity. SPU-2 and SPU-3 showed ionic conductivities value of 2.56×10^{-3} and 5.05×10^{-3} S/cm, respectively. The ionic conductivity is enhanced as the number density of ionic moieties increases on poly (urethane-urea) chain.

3.3. Quantum dots, quantum confinement effect and its optimization

The absorption features give information about the QDs or nanoparticle formation i.e., the band gap and the size distribution of the nanoparticles. The UV-visible absorption spectra (**Figure 3.3a**) of EDA caped CdS shows excitonic transition between 400-500 nm. However, additional absorption peaks are observed in ultraviolet range 230 - 260 nm. The absorption peaks 428, 437, 441 and 453 nm are observed for CdS-1, CdS-2, CdS-3 and CdS-4 at EDA concentration of 0.05, 0.1, 0.5 and 1M, respectively. In general bulk CdS shows absorption peak around 512 nm. The absorption peaks of caped CdS shows blue shifted absorption band which confirmed the chemical bonding of EDA with CdS particle. The blue shift is due to complexation or chelation of bidentate EDA molecule on CdS surface. It is evident that lower concentration of EDA shows efficient role in particle growth as compared to higher concentration EDA which predominantly shifted the absorption towards longer wavelength. The additional peaks get more resolved in ultraviolet region confirming destabilization effect of EDA or trap state in CdS particle. Interestingly, it can be depicted that EDA molecule can

control the size and surface quantization effect in particle. The direct band gaps 2.60, 2.66, 2.50 and 2.46 eV are estimated through the absorption edge in tauc's plot of caped CdS (**Figure 3.3b**). Further, it can be concluded that highly concentrated EDA molecule destabilize the particle's surface leading to aggregation of the particle to form bigger particle.

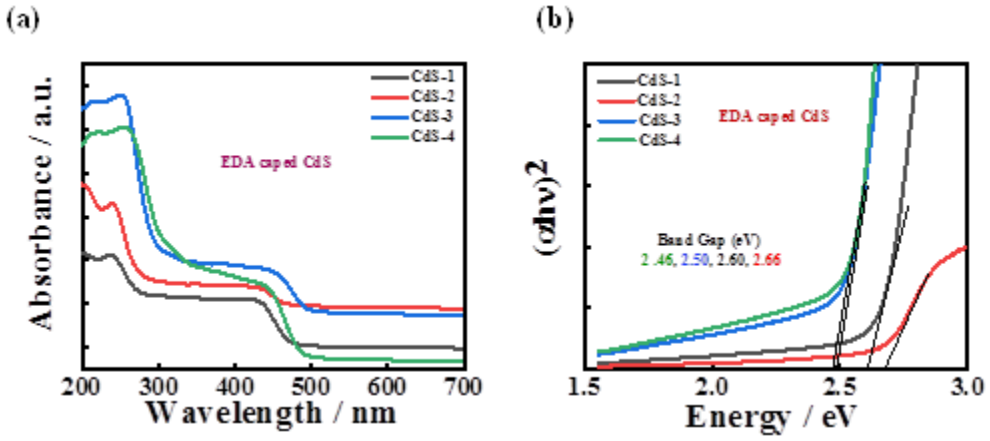

Figure 3.3: UV-visible absorption spectra of Ethylenediamine (EDA) caped CdS QDs to investigate extent of capping around CdS particle. (b) Estimation of direct band gap (Tau's plot).

The uncapped (bulk) CdS shows absorption peak around 460 nm while EDTA caped CdS exhibited absorption peak around 445, 428, 415, 405 and 397 nm for sample CdS-1, CdS-2, CdS-3, CdS-4 and CdS-5, respectively. Absorption spectra of capped / uncapped CdS quantum dots are shown in **Figure 3.4a.** The absorption peak of capped CdS shows a systematic blue shift with decreased concentration of sulfide ion at EDTA wrapped Cd^{2+} under constant concentration of capping solution. The possible direct transitions, $(\alpha h\nu)^2$ vs $h\nu$ is plotted and corresponding band gap were obtained from extrapolating the straight portion of the graph on $h\nu$ axis. The band gaps are extracted as 2.52, 2.60, 2.65, 2.69 and 2.71 eV for caped CdS samples (**Figure 3.4b**). The obtained values of the gap energy are higher than that of CdS bulk (2.42 eV) at room temperature. These values are shifted compared with the bulk value and this could be a consequence of a size quantization effect in the sample. Thus, the reduction in particle size is ascribed with blue shift in the optical band gap of the sample. The absorption spectrum of capped QDs shows a blue shift indicating a decrease in the size of the

particles. This is a consequence of capping surface with carboxylate groups chemisorbed on the surface due to the interaction of negative charged with Cd^{2+} rich surface.

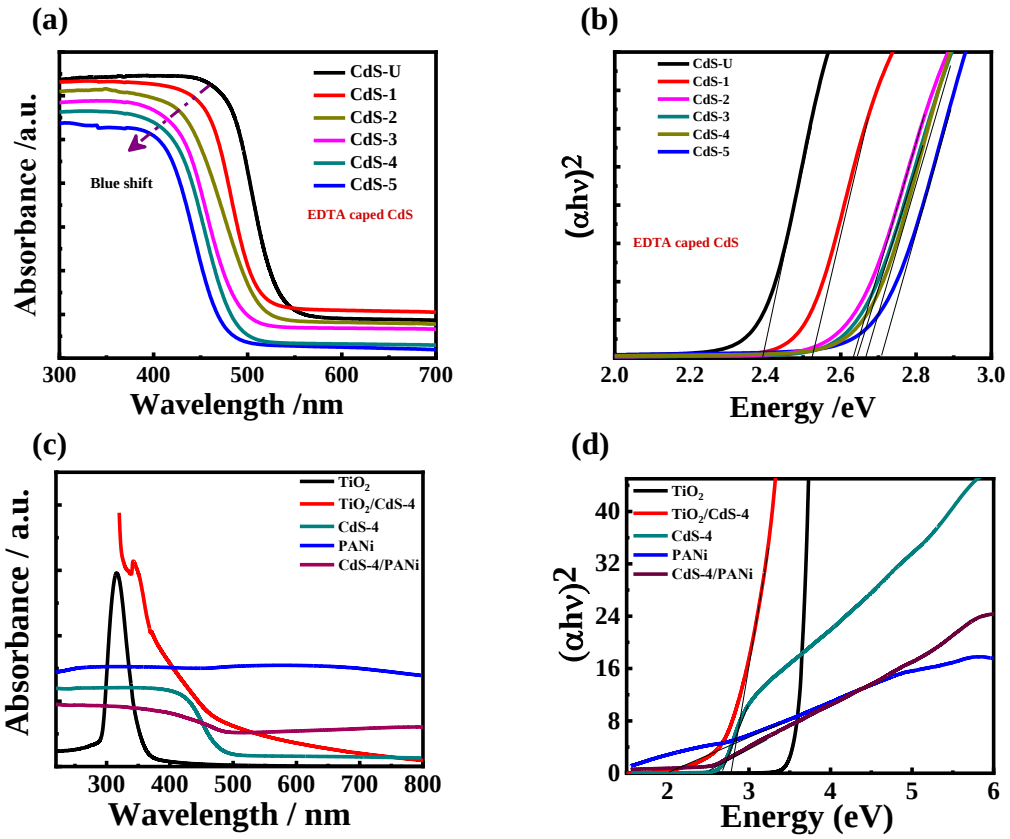

Figure 3.4: (a) UV-visible absorption spectra of various EDTA caped CdS solid thin film. (b) Tau's plot for estimation of direct band gap. (c) UV-visible absorption spectra of thin film on layered structure. (d) Tauc's plot for estimation of direct band gap.

UV—visible absorption spectra of TiO_2 film shows sharp (intense peak) at 317 nm at the ultraviolet region which instantly acts as photocatalyst (**Figure 3.4c**). The observed UV pattern indicate that TiO_2 particle react with deep UV that correspond to photocatalytic reaction. However TiO_2/CdS-4 shows red shifted excitonic transition around 344 nm indicating that layered structure are susceptible to harvest light correspond to near visible portion. The CdS-4 shows absorption band around 405 nm which indicates material can absorb visible light. Polyaniline (PANi) displays two absorption bands around 315 nm and 577 nm. The first absorption peak is due to presence of polaronic transition in conducting emeraldine salt (extent of HCl doping) while the second absorption bands arises from π - π*

electron transition within benzoid ring (extent of conjugation). The CdS-4/PANi shoes two absorption bands 335 nm and 793 nm and thus red shifting confirms the harvesting capacity of QDs towards visible light and PANi supports the absorption transition in QDs due to surface conduction. The red-shift in the UV-Vis spectra is related to the chemical bonding between CdS and PANi and thereby to the formation of bigger-size particles in the presence of PANi layer. The direct band gaps are estimated as 3.47, 2.56, 2.69, 2.00 and 2.51 eV for TiO_2, TiO_2/CdS-4, CdS-4, PANi and CdS-4/PANi, respectively (**Figure 3.4d**). The band gap is lowered down for layered structure and confirmed the harvesting capacity as visible portion of light. Thus, a red shift is observed in energy due to the quantum confinement phenomenon.

3.3.1. Electrochemical characteristics of capped CdS particle and PANi

EDA caped CdS clear oxidation and reduction peaks in cyclic voltammogram (**Figure 3.5a**). The onset potential of oxidation and reduction peaks are observed around - 0.80 and - 0.40V in caped CdS-1. And thus, onset peak to peak separation potential (ΔE_{pp}) is calculated as – 0.40V. The CdS-2 shows oxidation around - 0.70 V and reduction around - 0.33V and thus ΔE_{pp} = - 0.37V. CdS-3 shows redox behaviour around 0.18V and - 0.41V and ΔE_{pp} = 0.59V. Similarly, CdS-4 shows onset oxidation around – 0.76V and 0.10V and reduced around – 0.41V. The variation of oxidation and reduction potential is attributed with filling of surface states due to extent of interaction between CdS and capping molecule.

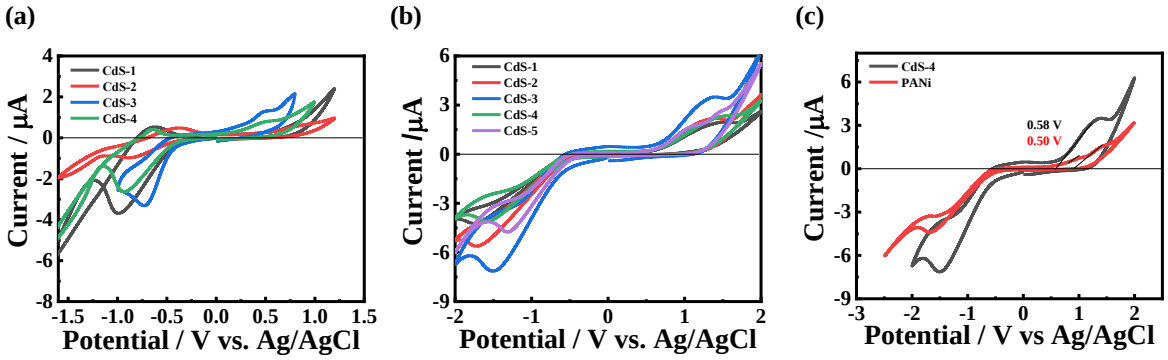

Figure 3.5: Electrochemical characteristic response: (a) Cyclic voltammetry measurement of EDA caped CdS at various concentration of capping agent. (b) Cyclic voltammetry of EDTA caped CdS through variation of concentration of Sulfide ion in EDTA caped CdS solutions with scan rate of 10 mV/s measured at room temperature**.** (c) Cyclic voltammetry of optimized EDTA caped CdS and PANi solution.

Sample	$[S^{2-}]$ [M]	λ_{max} (nm)	E_g (eV)	E_{ox} (V)	VB (eV)	CB (eV)
TiO_2	-	357	3.47	1.48	-5.88	-2.41
CdS-U	-	460	2.42	-	-	-
CdS-1	0.25	445	2.52	0.55	-4.95	-2.43
CdS-2	0.18	428	2.60	0.65	-5.05	-2.45
CdS-3	0.16	415	2.65	0.62	-5.05	-2.37
CdS-4	0.14	405	2.69	0.58	-4.98	-2.29
CdS-5	0.11	397	2.71	0.60, 0.82	-5.00, -5.12	-2.29, -2.51
PANi	-	317, 577	2.00	0.50	-4.90	-2.90

Table 3.2: UV-visible and electrochemical parameters and its values for photocatalyst, EDTA caped CdS QDs and PANi

In other hand, EDTA caped CdS shows clear oxidation and reduction with complete reversible reaction **(Figure 3.5b**). The physical parameter has been listed in **Table 3.2**. CdS-1 shows onset oxidation potential around 0.55V and reduction around – 0.49V causing onset peak to peak separation potential ΔE_{pp} = 1.04V. Similarly, CdS-2 exhibits oxidation and reduction around 0.65V and -0.30V leads to ΔE_{pp} = 0.95V. CdS-3 shows oxidation around 0.62V and reduction around – 0.51V result in ΔE_{pp} = 1.13V. Similarly, 0.58V and -0.49V are assigned to oxidation and reduction in CdS-4 . The onset peak to peak separation potential is calculated to be 1.07V. However, CdS-5 shows double oxidation around 0.60 and 0.82V and complete reduction occurred around -0.43V. The onset peak to peak separation potential is calculated as 1.03 and 1.25V due to both oxidations. The variation of potentials is corresponds to change in the surface state. PANi exhibits two consecutive oxidation around 0.50V and 0.87V and completely reduced around -0.57V (**Figure 3.5c)**. It is concluded that double oxidation confirms the different surface state which can be used to mobilize the photoexcited electron and activate the deactivated electron in QDs.

3.3.2. Extent of interaction, chemical capping and particle size response of CdS

The bulk band gap of CdS is 2.42eV. The formation of CdS QDs is due to optimum interaction of EDTA capping materials with the surface of CdS particle. SEM morphological investigation clearly depicts the formation of large particle (nanoparticle) in uncapped or bulk CdS (**Figure 3.6a)**. Capping agent has been used to cover up the nascent nucleus to control the size of quantum dots. SEM images of uncapped and EDTA capped CdS are shown in indicating significantly smaller particle dimension in capped system (40 nm) as compared to uncapped CdS (130 nm). Usually, larger particle in uncapped CdS are formed in some sort of cubical shape while EDTA surface stabilized CdS shows almost uniformly distributed grains of spherical shape. AFM image (**Figure 3.6b**) of EDTA capped CdS exhibits spherical particle dimension with average roughness value of 19 nm while TEM image (**Figure 3.6c**) clearly indicate tiny nanoparticle of average size of 4 nm. The distribution of nanoparticle is shown in the inset image indicating the particle distribution from 2 to 5 nm. This is to mention that smallest particle is observed through TEM, where the sampling is made from a very dilute dispersion, but the agglomerated dimension is visible in SEM and AFM micrographs. Ultrafine suspensions of various capped CdS nanoparticles are prepared in absolute ethanol through ultra sonication for dynamic light scattering (DLS) measurement based on the random thermal motion or Brownian motion to measure the relative particle dimension (**Figure 3.6d**). Different extent of Sulphur ions generate particle sizes of 14, 11 and 8 nm of CdS nanoparticle from 0.16, 0.14 and 0.11 M concentration of sodium sulfide in the solution of EDTA capped Cd^{+2} ions. This is worth mentioning that DLS measures the hydrodynamic size of the particles which is apparently bigger than the particle size observed through TEM. However, it is evident that nanometer dimension CdS particles are formed using optimized sulfide ion and EDTA as capping agent. Quantum confinement effect can be also proved by FTIR spectra (**Figure 3.6e**). In the higher energy region of FTIR spectrum of bulk CdS, the peak at 3483 cm^{-1} is assigned to O-H stretching of absorbed water on the

surface of CdS. The presence of water is confirmed by its bending vibration at 1635 cm^{-1}. The peak at 1435 is assigned to bending vibration of ethanol used in the synthesis process. The C-O stretching vibration of absorbed ethanol gives its weak peak at 1094 cm^{-1}. The weak band around 810 cm^{-1} in bulk CdS is attributed to the Cd-S bond. The peaks around 3033 cm^{-1} are assigned to asymmetric vibration of $-CH_2$ group in EDTA molecule. Similarly, the peak 2909 cm^{-1} is assigned to asymmetric vibration of $–CH_2$ group in EDTA-CdS. The vibrational energy shifted towards lower energy which confirms the interaction of EDTA with CdS leads to quantum confinement effect. The peaks around 3525 and 3383 cm^{-1} are attributed to Hydrogen bonded –OH and –NH stretching vibration in EDTA molecule. In other hand, the broad peak 3481 cm^{-1} confirms the presence of –NH group in EDTA caped CdS. The peak value shifted towards higher energy because of absence of –OH group and reduction of hydrogen bond on EDTA caped molecule. In addition, the peak around 1728 cm^{-1} confirmed the presence of –CO group (Carboxylate ion) in caped CdS and the vibration frequency is little higher than the 1691 cm^{-1} in EDTA molecule. The shifted value also shows an evidence of reduced hydrogen bonding and indicates abundant carboxyl groups are tethered on the surface of CdS. Other peaks are as usual sharp and intense and decrease in peak intensity confirms the capping effect of EDTA around CdS particle. Thus, EDTA avoids nanoparticles to coagulate and agglomerate due to stabilization effect.

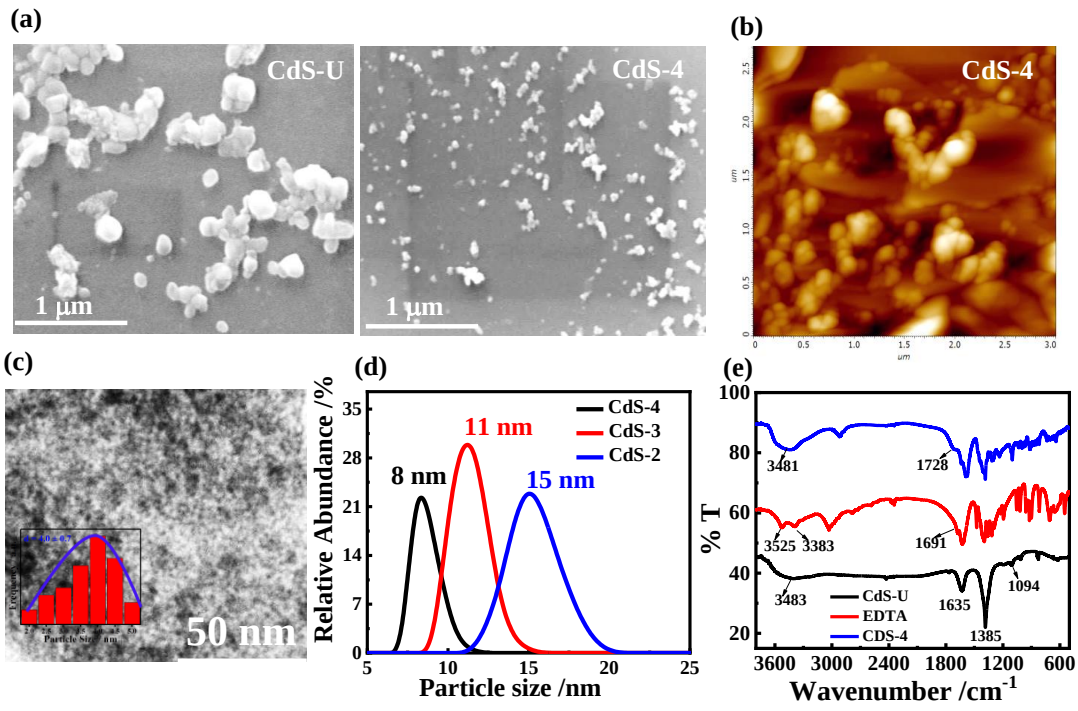

Figure 3.6: (a) SEM image of uncapped CdS and EDTA caped CdS. SEM revealed that capping reduced the agglomeration as a result little homogeneous distribution of particle.(b) AFM image of caped CdS nanoparticle. (c) TEM image of EDTA caped CdS QDs with inset histogram of particle size distribution. Image displayed spherical particle distribution with maximum size range 4 ± 0.7 nm. (d) DLS measurement of EDTA caped CdS QDs showing solvated dynamic size as 8, 11 and 15 nm for different band gap particle.(e) FTIR spectra of uncapped CdS , EDTA and EDTA caped CdS.

3.4. Fabrication of QDSS cells and its solar (light) energy conversion response

Quantum dot sensitized solar cell was developed through assembly of photoanode FTO/TiO_2/CdS, ionomer electrolyte matrix and counter electrode (Pt). The proper alignment of interfacial energy levels drives the photoexcited excitons in desired direction to initiate photovoltaic reaction in device.

3.4.1. Energy levels, photo sensitization and photovoltaic charge transfer phenomenon

The bulk CdS band gap is 2.42eV. Photo sensitization is due to absorption of photon energy which leads to generation of photoexcited electron and hole in the layer of Quantum dots [139]. The extent of conversion of solar energy into electrical energy depends on proper alignment of energy levels between different constituent layers in QDSS cells. HOMO energy levels from electrochemical measurements and LUMO energy levels calculated from

optical energy gap are combined to draw energy diagram which can explain the flow of electron and hole in proper direction. Optimum functionality stabilizes the energy levels in polyurethane ionomer. It is evident that the close proximity of valence band of CdS-4 and HOMO level of SPU-3 ionomer gel allows the holes to pass on to electrode (Pt) easily. On the other hand, similar energy level of conduction bands of CdS-4 and photocatalyst TiO_2 (E_{VB} = -5.88eV, E_{CB} = -2.41eV) help transportation of electron towards electrode (FTO, WF = - 4.4 eV), as shown by the arrows. This is worth mentioning that conduction band of CdS-4 and LUMO energy level of SPU-3 ionomer gel are also quite similar which may allow the electron to flow in a reverse direction toward Pt electrode and thereby jeopardize the charge carrier transportation for solar cell activity. In order to circumvent the problem, a polymer layer [polyaniline, E (HOMO) = 4.90eV, E (LUMO) = 2.90 eV] is added in between CdS and SPU-3 whose LUMO level is quite different than that of ionomer gel or EDTA caped CdS and thereby this buffer layer will not allow the electron to pass on to Pt (WF = -5.00eV) electrode and instead it will puss the electron only towards other direction (FTO electrode through TiO_2). PANi improves interfacial conductivity via formation of intermolecular hydrogen bond through EDTA caped CdS and SPU-3 ionomer gel. The direction of electron transport and hole transport has been shown in **Scheme 3.2**. Based on the energy values, it will activate the deactivated electrons which dropped from QDs and TiO_2 in the layer structure to maintain the reversibility of solar energy conversion activity.

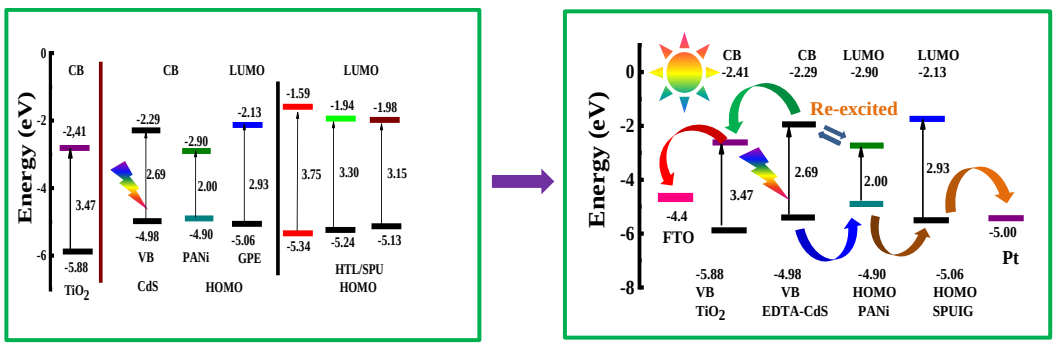

Scheme 3.2: HOMO-LUMO energy levels of sulfonated polyurethane and its alignment with band structure of TiO_2 and CdS quantum dots. Photosensitization and charge transport mechanism with hole conducting sulfonated polyurethane gel matrix.

3.5. Photovoltaic reaction and hole conduction mechanism in QDSS cells

Photovoltaic reaction can be realized through fabricating device with layer structure on electrodes and inserting electrolyte matrix between photoanode and counter electrode (**Figure 3.7a**). The structural designed device FTO/TiO_2/CdS-3/Liquid SPU-1/Pt/FTO showed photocurrent density (J_{SC} = 0.01mA/cm^2 and photovoltage (V_{OC} = 0.434 V) in the dark state of device (**Figure 3.7b**). However, same structural device exhibited little enhanced J_{SC} = 0.09mA/cm^2 and efficient photovoltage (V_{OC} = 0.78V). Photovoltaic reaction has been shown in **Scheme 3.3**. Photovoltage is related to functioning behaviour of electrolyte matrix. The high V_{OC} indicates that electrolyte matrix functioned perhaps due to some structural and reversible change in redox active pendant group of polyurethane ionomer electrolyte. Photovoltaic reaction occurred perhaps because of recharging phenomenon on the photooxidised QDs through ionic conduction behaviour of solution phase ionomer electrolyte matrix.

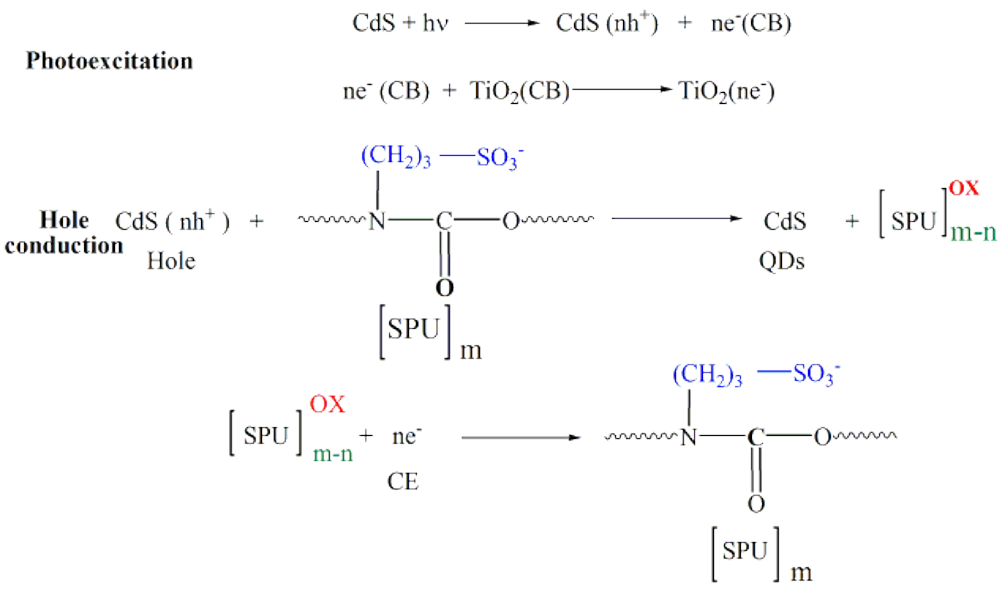

Scheme 3.3: Schematic mechanism of photovoltaic reaction in QDSS cell through redox active ionomeric segments.

Polyurethane ionomer (SPU-1) was developed as gel phase for substituting electrolyte solution matrix. The device FTO/TiO_2/CdS-3/ SPU-1/Pt/FTO showed change of J_{SC} = 0.10 mA/cm^2 and V_{OC} = 0.665V through gel phase of electrolyte (**Figure 3.7c**). Similarly, same device structure showed more solar characteristic curve through SPU-2 ionomer gel with J_{SC} = 0.09, V_{OC} = 0.660V, FF = 0.33 and η = 0.02%. These data demonstrates improved interfacial wettability and charge transport due to little higher level of functionalization on hard segment content of SPU-2. The device structure FTO/TiO_2/CdS-4/ SPU-3/Pt/FTO showed enhanced solar characteristic values J_{SC} = 0.92 mA/cm^2, V_{OC} = 0.520V, η = 0.10% through next higher level of sulfonation in SPU-3 (**Figure 3.7d**). The variation in solar parameters is due to structural and quantum confinement effect in CdS QDs and polyurethane ionomer. Further, FTO/TiO_2/CdS-4/ SPU-4/Pt/FTO showed photovoltaic curve with J_{SC} = 0.28 mA/cm^2, V_{OC} = 0.430V, η = 0.007% while FTO/TiO_2/CdS-4/RGO/SPU-4/Pt/FTO displayed a curve with J_{SC} = 0.20, V_{OC} = 0.450V and η = 0.011% (**Figure 3.7e**). In former case, there is possible charge recombination with internal trap state in SPU-4 due to presence of two different energy gaps. Therefore, Surface dopant RGO has been introduced between CdS-4 and SPU-4 to minimize the energy barrier for efficient charge transport. In later case, little high V_{OC} confirms that reversible charge transport occurs through redox active environment of SPU-4 ionomer gel. However, interfacial aggregated state lowers down the current density. In general, the lower cell parameter values for QSDSSC is due to the restriction offered by the hydrophobic content and hydrogen bonded polymeric network to the transfer and transport reactions within the electrolyte active group of polyurethane ionomer and also the poor wetting of the photoanode. It also suggested that an optimum level of functionalization on hard segment content of SPU may improve the reversible function of photovoltaic redox reaction.

The possible trap states (recombination center in QDs or SPU) have been minimized via introduction of RGO, CB and PANi between photoanode and ionomer electrolyte matrix. Interfacial dopants enhance the electrical conduction through minimization of internal energy barrier. Surface dopants may intensify hole conduction. Since sulfonation improves the adhesion and electrical conduction of ionomeric content via hydrophilic properties in SPU. Photovoltaic parameters are shown in **Table 3.3.**

Highly sulfonated SPU-3 (Eg = 2.93 eV) polyurethane ionomer gel was developed to investigate photovoltaic reaction with interfacial dopants. The device FTO/TiO_2/CdS-4/RGO/SPU-3/Pt/FTO showed J-V characteristic curve with J_{SC} = 0.53 mA/cm^2, V_{OC} = 0.540V, η = 0.04%. The J-V curves and power vs. voltage plot have been shown in **Figure 3.8a, b.** Photovoltaic conversion efficiency further lowered down likely due to interfacial aggregation which slows down the kinetics of photovoltaic redox reaction leading to high charge recombination. Further, a thin layer of carbon black (CB) was inserted in place of RGO and fabricated device exhibited J_{SC} = 2.74 mA/cm^2, V_{OC} = 0.34V and η = 0.25%. The device parameter values indicate that photocurrent density is enhanced probably due to increased injection of extent of photoexcited charge into conduction band (CB) of TiO_2. This lower V_{OC} is probably because of the inefficient reduction of hole by the sulfonate segment in the ionomer electrolyte. In other hand, V_{OC} is decreased indicating retardation in redox behaviour of ionomer electrolyte matrix [140]. Photovoltaic parameters have been shown in **table 3.4**

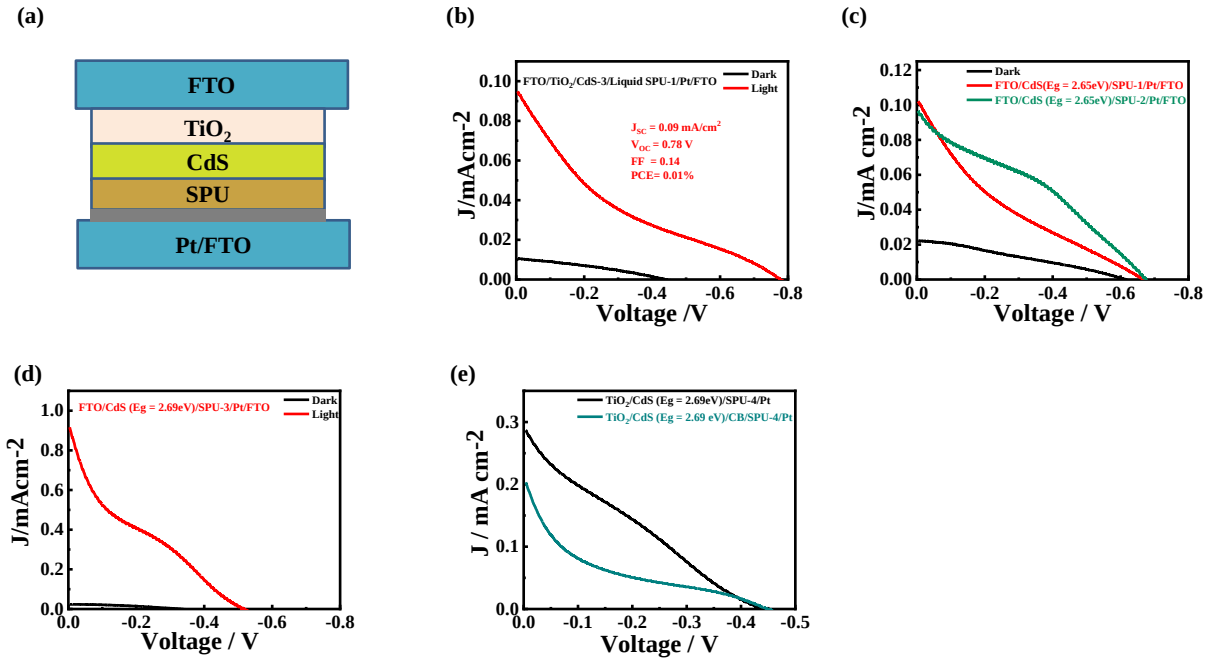

Figure 3.7: (a) Room temperature fabrication and layered assembly of Photoanode, polyurethane ionomer gel and counter electrode. (b) J-V characteristic curve of QDSS cell through photosensitization FTO/TiO_2/CdS-4 using liquid ionomer electrolyte (SPU-1) in DMSO.(c) J-V characteristic measurement (In dark and light) of QDSS cell using polyurethane ionomer gel (SPU-1 and SPU-2) through photosensitization of FTO/TiO_2/CdS (Eg = 2.65 eV). (d) Photovoltaic response (J-V curve) of QDSS cell using CdS (Eg = 2.69eV) and SPU-3 ionomer gel. (e) J-V characteristic measurement of QDSS cell via photosensitization of FTO/TiO_2/CdS-4 and FTO/TiO_2/CdS-4/CB (carbon black) electrode using SPU-4 ionomer gel.

Gel matrix	Photoanode FTO/TiO1/QDs	Eg (QDs)	J_{SC} mA/cm^2	V_{OC} (V)	FF	PCE (%)
SPU-1	CdS-3	2.65	0.10	0.665	0.15	0.010
SPU-2	CdS-3	2.65	0.09	0.660	0.33	0.020
SPU-3	CdS-4	2.69	0.92	0.520	0.21	0.100
SPU-4	CdS-4	2.69	0.28	0.430	0.06	0.007
SPU-4	CdS-4	2.69	0.20	0.450	0.11	0.011

Table 3.3: Influence on photovoltaic parameters via tuning HOMO-LUMO energy levels of sulfonated polyurethane under different size or band gap Quantum dots as photosensitizer

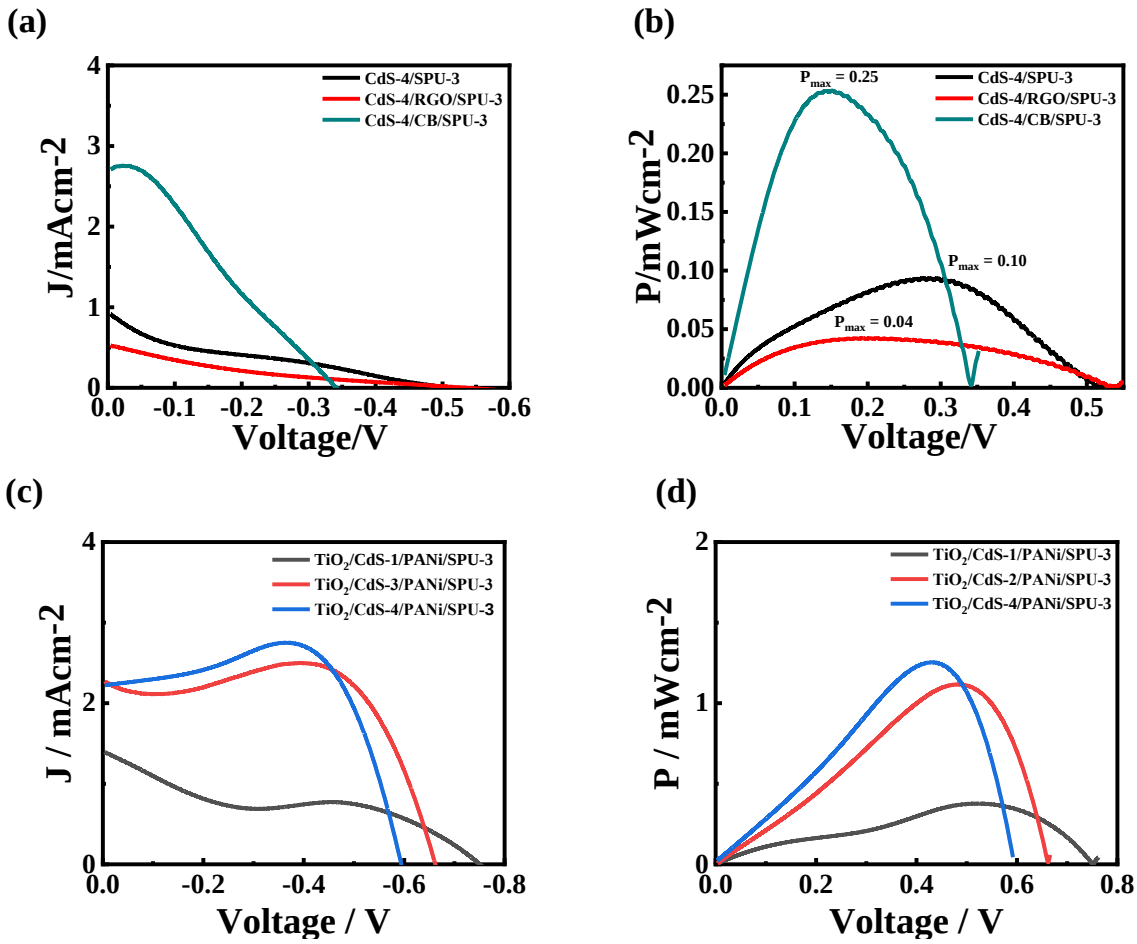

Figure 3.8: (a) J-V characteristic curve of QDSS cells through variation of interface structure between FTO/TiO_2/CdS-4 and SPU-3 ionomer gel.(b) solar energy conversion characteristic curves. (c) Photovoltaic J-V characteristic curve of QDSS cells using SPU-3 ionomer gel and influence of quantum confinement effect in CdS QDs. (d) Solar energy conversion characteristic plots for estimation of efficiency.

Structure of QDSS cells	J_{SC} mA/cm^2	V_{OC} (V)	FF	η (%)
FTO/TiO_2/CdS-4//SPU-3/Pt/FTO	0.92	0.52	0.21	0.10
FTO/TiO_2/CdS-4/RGO/SPU-3/Pt/FTO	0.53	0.54	0.14	0.04
FTO/TiO_2/CdS-4/CB/SPU-3/Pt/FTO	2.74	0.34	0.27	0.25
FTO/TiO_2/CdS-4/PANi/SPU-3/Pt/FTO	2.20	0.60	0.94	1.25

Table 3.4: Structure of Quantum dot sensitized solar cell consisting of optimized sulfonated polyurethane ionomer gel (matrix). The photovoltaic physical parameter and its values are calculated accordingly under photoillumiation with 100 mW/cm^2 intensity of light operated at room temperature

Photosensitizer	Electrolyte matrix	J_{SC} mA/cm^2	V_{OC} (V)	FF	η (%)
CdS-1	SPU-3	1.15	0.750	0.36	0.38
CdS-2		2.27	0.660	0.74	1.11
CdS-4		2.20	0.600	0.94	1.25

Table 3.5: Size quantization effects of CdS QDs on photovoltaic parameters and its values measured at constant hole conducting layer or hole conducting electrolyte

Finally, hydrochloric acid (HCl) doped conducting polyaniline was inserted in place of carbon black to improve interfacial transfer phenomenon. Photovoltaic reactions were investigated with different size or band gap developed CdS QDs. First, device FTO/TiO_2/CdS-1/PANi/SPU-3/Pt exhibited J_{SC} = 1.15 mA/cm^2, V_{OC} = 0.75V and η = 0.38% (**Figure 3.8c**). Power vs. voltage plot has been shown in **Figure 3.8d**. The high V_{OC} might be due to efficient hole conduction which may be facilitated through interfacial conducting channel of polyaniline. However, saturation current density deviated positively from solar characteristic curve leading to spike which may be because of slight photoexcitation from internal trap states in QDs [141]. Similarly, photo illuminated device FTO/TiO_2/CdS-3/PANi/SPU-3/Pt showed marked change in photovoltaic parameter values. The device exhibited J_{SC} = 2.27mA/cm^2, V_{OC} = 0.660V and η = 1.11%. However, steady state (saturation) current density first decreases and then slightly increases probably due to little charge recombination on surface of QDs. The device FTO/TiO_2/CdS-4/PANi/SPU-3/Pt showed J_{SC} = 2.20 mA/cm^2, V_{OC} = 0.600V, FF = 0.94 and η = 1.25%. Saturation current density still deviated negatively which stabilize at 2.20 mA/cm^2. Highly sulfonated polyurethane ionomer showed irregular J-V curve which might be probably due to phase mixing phenomenon in polyurethane ionomer. The deviation in solar characteristic curve may be due to insulating properties of capping ligand concentrated around QDs. This may cause slight hindrances in reversible charge transport. Thus, quantum dots confinement effect play

critical role in photovoltaic reaction and functionalization level affects the photovoltaic redox reaction and hence sustainable conversion efficiency **(Table 3.5).**

3.6. Conclusions

In summary, polyurethane ionomer was developed through incorporating short chain alkyl sulfonate in hard segment content of polyurethane chain. UV-visible absorption spectra revealed red shifting in absorption peak which confirms the presence of new chromophore in polyurethane chain. Short chain alkyl sulfonate controlled the energy gaps due to structural stabilization efficiency in polyurethane chain. Polyurethane ionomer showed efficient thermal stability. Polyurethane ionomer showed electrochemical redox activity in solution phase. Energy levels and energy gaps showed efficient change and varied with functionalization level either in QDs or Polyurethane ionomer. The increases in ionomeric content improved electrical conduction in redox active environment for efficient charge transport. Photovoltaic reaction was realized successfully in QDSS cells. Photovoltaic redox reaction was confirmed through variation of photovoltage in fabricated device. Highly sulfonated polyurethane ionomer showed approximate solar characteristic curve in QDSS cells. The resultant QDSSC showed a power conversion efficiency of 1.25% via efficient electrolyte activity of poly (urethane-urea) ionomer.